Effect of Sodium Addition and Thermal Annealing on Second-Order Optical Nonlinearity in Thermally Poled Amorphous Ta_2O_5 Thin Films

Amy S. K. Tong,[1, a)] Flavie Bondu,[2, a)] G. Senthil Murugan,[1] James S. Wilkinson,[1] and Marc Dussauze[2]

[1]Optoelectronics Research Centre, University of Southampton, Southampton, SO17 1BJ, UK

[2]Institut des Sciences Moléculaires, Université de Bordeaux, 33400 Talence, France

We demonstrate second-order optical nonlinearity (SON) induced in amorphous tantalum pentoxide (Ta_2O_5) films by thermal poling. The effects of sodium addition and thermal annealing on the efficiency and stability of second harmonic generation (SHG) have been investigated. Maker fringe analysis have been used to quantify the poling-induced SON. $\chi^{(2)}$ of 0.46±0.02 pm/V and 0.34±0.02 pm/V was achieved for sodium-containing and pure Ta_2O_5 films, respectively. Both the strength and the temporal stability of the induced nonlinearity are discussed with respect to the poling mechanisms and measured electrical conductivity. The lower density of uncombined charges of the Ta_2O_5 thin films is believed to play a role in the strength of SHG signal and the rate of SHG decay decreases with thermal annealing.

I. INTRODUCTION

Photonic circuits provide a route to highly functional low-cost optoelectronic and all-optical devices, and are a field of rapid commercial growth. In particular, silicon-on-insulator (SOI) waveguide technology offers high performance with standard wafer processing, for mass-market applications.[1] Recently, dielectric waveguides on silicon have shown enhanced performance for nonlinear processes, particularly due to low two-photon absorption at telecommunications wavelengths and wideband optical transparency.[2] Thin film dielectric waveguides exploit existing silicon process technology and complement SOI waveguides in multilayer silicon photonic circuits or all-dielectric circuits.[3] As in integrated electronics, functionalities such as gain, all-optical and electro-optic switching, feedback and frequency filtering are needed to realize a full range of circuit capability, and dielectric waveguides may complement SOI waveguides in providing these functions. However, amorphous dielectric films do not exhibit the second-order optical nonlinearity required to achieve efficient electro-optic switching, known as the Pockels effect, due to lack of average non-centrosymmetry.

Second-order optical nonlinearity (SON) is essential for many optical processes such as electro-optic modulation, second harmonic generation (SHG), sum and difference frequency generation, and optical parametric

[a)] A.S.K. Tong and F. Bondu contributed equally to this work.

oscillation. SON naturally exists in crystals with non-centrosymmetric structure and has been induced in glasses by the process of thermal poling.[4] Thermal poling consists in applying a DC electric field to a heated sample creating charge dissociation and moving cations through the glass. The sample is then brought back to room temperature to freeze the charges in place, creating a frozen-in electric field. This frozen-in electric field, E_f, then acts upon the third-order susceptibility ($\chi^{(3)}$) inherent in the material to create an effective second-order susceptibility, $\chi^{eff(2)}$, through $\chi^{eff(2)} = 3E_f\ \chi^{(3)}$. Clearly, to achieve high $\chi^{eff(2)}$ a material must demonstrate a combination of high $\chi^{(3)}$ and the ability to sustain a high frozen-in electric field, which relates in a first approximation to a high dielectric breakdown strength.

Towards this end, glass systems with high third-order nonlinearity such as niobates [5], tellurites [6, 7], or germanates [8] for oxides and also arsenic or germanate sulphide for chalcogenide compositions, have been explored. To date, promising results have been obtained for heavy metal oxide (HMO) systems with stable second-order nonlinear optical coefficient ($\chi^{(2)}$) values reported in the range 1-10 pm/V [5] and also for poling of chalcogenides, though the latter have issues in the stability of the induced nonlinearity.[9, 10, 11, 12, 13]

The literature on poled amorphous thin films is less abundant and mainly focuses on various kinds of silica film [14, 15, 16] with additional reports on HMO systems.[17] These studies have demonstrated the possibility of transferring the poling process from bulk to thin film forms. Finally, examples of electro-optical devices [18, 19] or frequency convertors based on thermally poled glasses have also been demonstrated.[20] On SiO_2 films, Fage-Pedersen et al. [21, 22] have obtained the best frequency conversion performance with a normalized conversion efficiency of $1.4x10^{-3}$ %/W/cm^2 using periodic electrodes to obtain a high periodic contrast of the inbuilt static field. The effective second-order optical response in this device was $\chi^{eff(2)} = 0.13$ pm/V which is comparable to the efficiency observed in a similar bulk glass. Nevertheless, up to now, practical applications of thermally poled glassy materials have been limited, mainly due to their unfavorable comparison with the very high second-order optical coefficients exhibited by ferroelectric crystals such as $LiNbO_3$.

Silicon nitride (Si_3N_4), aluminum oxide (Al_2O_3) and tantalum pentoxide (Ta_2O_5) are three leading candidates for integration of dielectric waveguides on silicon, due to their silicon process compatibility and high refractive index, leading to potential for compact devices. High $\chi^{(3)}$ without two-photon absorption has been exploited in Si_3N_4 and Ta_2O_5 waveguides [2, 23] and gain or lasing from rare-earth doping has been demonstrated in Al_2O_3 [24, 25] and Ta_2O_5 waveguides.[26, 27] Recently, higher values of $\chi^{(3)}$ [28, 29] and extremely low losses [30] have been demonstrated in Ta_2O_5 waveguides, when compared with Si_3N_4 waveguides, rendering them competitive among these thin-film

materials. To date, demonstrations of induced $\chi^{(2)}$ in these materials have been limited to Si_3N_4 thin films, where 5 pm/V has recently been achieved on an unpoled, silicon-rich sample.[31] The high $\chi^{(3)}$ of Ta_2O_5 combined with comparable electrical breakdown strength and its use as a highly insulating high-k gate dielectric in CMOS transistors [32] offers the promise of Ta_2O_5 poled waveguides exhibiting higher electro-optic coefficients than those demonstrated to date in other amorphous materials. Furthermore, while $LiNbO_3$ and Si_3N_4 only transmit up to wavelengths of about 5 μm, HMO such as Ta_2O_5 transmit light at wavelengths up to about 8 μm [33], opening up opportunities for switchable and tunable devices in the mid-infrared.

While Ta_2O_5 appears to be a promising candidate for thermal poling, process conditions for poling and the resultant SON have yet to be established. In this paper, we report a quantitative study of induced $\chi^{(2)}$ in thermally poled Ta_2O_5 thin films deposited on borosilicate glass substrates. The stability of the SON response was also investigated over more than 1300 hours for all samples. The influence of sodium addition and annealing of Ta_2O_5 thin films on the poling-induced $\chi^{(2)}$ and stability is discussed. A study of the electrical resistivity of Ta_2O_5 thin films was performed to further understand the effect of sodium addition and thermal annealing on the SHG signal. The combined charges and the electrical charge relaxation on the strength and stability of the SON response of the Ta_2O_5 thin films are discussed.

II. EXPERIMENTAL

A. Thin film deposition

Films of 4 μm thickness were deposited on Schott Borofloat 33 glass substrates (25×15×1 mm), and also on silicon substrates for ellipsometry measurements. Schott Borofloat 33 substrates were chosen to match the conductivity of the thin film. The films were deposited using radio frequency (RF) sputtering (Oxford Instruments Plasmalab System 400), from 6" diameter powder-pressed targets of compositions Ta_2O_5 or $0.95Ta_2O_5$-$0.05Na_2O$ (in mol% noted as Na:Ta_2O_5 in the rest of the article). The targets were prepared in a dry, inert atmosphere. The deposition was performed under an oxygen/argon atmosphere (oxygen flow 5 sccm, argon flow 20 sccm and pressure 10 mTorr) at an RF power of 300 W with the substrate maintained at 200 °C. These parameters had previously been found to represent the optimal conditions to give low loss in Ta_2O_5 based slab waveguides.[34] Half of the films were annealed at 500 °C for 3 hours under an oxygen atmosphere to relieve any stress built up in the films [35] and to replenish the oxygen, which is depleted during the sputtering process.

B. Thin film characterization

This manuscript was accepted by J. Appl. Phys. Click here to see the version of record.

The thickness of the deposited films was determined using a stylus profiler (KLA Tencor P16). The film thicknesses were found to be within ±10% of the targeted 4 μm thickness. The refractive indices of the films were measured using an ellipsometer (J.A. Woollam M-2000) at wavelengths between 500 and 1600 nm. X-ray diffraction (XRD) was used to study the crystallinity of annealed/unannealed Na:Ta_2O_5 and Ta_2O_5 films.

C. Electrical properties of films

To understand the conduction mechanism of the Na:Ta_2O_5 and Ta_2O_5 films, impedance measurements were conducted on a bare Borofloat 33 substrate, using an impedance analyzer (Solartron 1260). 1 cm × 2 cm electrodes were formed from high conductivity silver epoxy paste on the front and back of the sample, and impedance measurements were performed at temperatures ranging from 200 to 300 °C. Nyquist plots of all samples at all temperatures were used to determine their DC resistance. To determine the resistance of the thin Ta_2O_5 films, the resistance of the Borofloat 33 substrate is removed from the total resistance of the sample, and the resistivity calculated using measured film thickness and electrode area.

D. Thermal poling

Thermal poling was performed in an inert atmosphere (flow of N_2) to provide blocking anode conditions avoiding protonic injection. Glass samples were heated from room temperature to the poling temperature, which was fixed at 300 °C for this study. Samples were poled by applying a voltage of either 1.3 kV or 2.0 kV for 30 minutes. Samples were cooled down to room temperature and the applied voltage was then removed. A schematic diagram of the apparatus used for thermal poling is shown in Fig. 1.

E. Depth distribution of the SON layer

Micro-SHG measurements were recorded in backscattering mode from a cut cross-section of the poled region using a confocal microscope, in order to determine the spatial distribution of the SON through the film and substrate. A picosecond laser operating at 1064 nm was used for measurements with a classical linear polarization. Both 1064 nm excitation and second harmonic collection were through a 50× microscope objective lens with a numerical aperture of 0.5. The in-plane spatial resolution is estimated to be 1.5 μm.

F. Maker fringe measurements of $\chi^{(2)}$

Maker fringes were recorded using a nanosecond laser operating at 1550 nm. For all experiments, a maximum energy of 100 μJ was applied to the sample. The pulse width was about 20 ns and the repetition rate of the laser pulses was 100 Hz. The intensity of the fundamental was monitored for each measurement and the generated second harmonic (SHG) signal was recorded using a photomultiplier and averaged over 64 laser pulses. Three

measurements were carried out. First, θ-scans were recorded using p-polarized incident beam and p-polarized or s-polarized transmitted second harmonic beam with θ being the angle of incidence between the laser beam and the normal to the sample surface. Second, ψ-scan were recorded with a p-polarized transmitted second harmonic beam at an angle θ = -64° corresponding to the maximal SHG signal for p-p polarized θ-scans. Third, SHG kinetics measurements were recorded on each sample using p-polarized incident beam and p-polarized transmitted second harmonic beam at θ = -64° as a function of time, to study SON stability.

III. RESULTS

A. Refractive index, dispersion and structure

The ellipsometry measurements of refractive index for the annealed and unannealed Na:Ta_2O_5 and Ta_2O_5 films are shown in Fig. 2.

Fig. 2 shows that the refractive index of the Na:Ta_2O_5 films is higher than that of the Ta_2O_5 films for both annealed and unannealed samples, as also seen in glasses.[36] The annealed films showed lower refractive index than the unannealed films, due to the replenishment of oxygen in material during annealing, as observed previously.[34]

Maker fringe measurements are performed with a pump wavelength of 1550 nm and an SH wavelength of 775 nm, so the refractive index values at these wavelengths extracted from the data in Fig. 2 are used for the Maker fringe calculations, described in section III D, are given in Table I.

TABLE I. Refractive indices of Ta_2O_5 films at the Maker fringe wavelengths

	1550 nm	*775 nm*
Unannealed Na:Ta_2O_5	2.083	2.116
Annealed Na:Ta_2O_5	2.077	2.106
Unannealed Ta_2O_5	2.056	2.099
Annealed Ta_2O_5	2.048	2.086

The XRD measurements of the annealed/unannealed Na:Ta_2O_5 and Ta_2O_5 films are shown in Fig. 3. Ta_2O_5 has been shown to be amorphous if annealed below 660 °C, becoming polycrystalline if annealed at higher temperatures.[37] Fig. 3 shows that our films are broadly amorphous but there may be nanocrystalline regions within the overall amorphous matrix.

B. Electrical properties of films

The DC resistance of the Borofloat substrates was found to vary between 0.60 and 0.76 MΩ as the temperature increased from 25 to 300 °C. Estimation of film resistivity at temperatures below 200 °C was not possible due to the high resistance of the samples. Table II shows the resistivities of the Ta_2O_5 films at temperatures 200 and 300 °C.

TABLE II. Resistivity (Ωm) extracted from impedance measurements of 4 µm unannealed and annealed Na:Ta_2O_5 layers, and unannealed and annealed Ta_2O_5 layers performed at 200 and 300 °C

	Unannealed Na:Ta_2O_5	*Annealed Na: Ta_2O_5*	*Unannealed Ta_2O_5*	*Annealed Ta_2O_5*
200 °C	1.11×10^9	4.24×10^9	7.14×10^9	1.15×10^{10}
300 °C	2.75×10^7	6.92×10^7	1.04×10^8	1.80×10^8

The resistivity of all films decreased with increase in temperature, as expected in insulators. The resistivity of the Na:Ta_2O_5 material is lower than for a Ta_2O_5 composition, for both annealed and unannealed films, due to the presence of mobile cations. The annealed films show higher resistivity than their unannealed counterparts, in both the Na:Ta_2O_5 and Ta_2O_5 cases. Annealing reduces the oxygen vacancies in the film, thereby reducing potential routes for conduction.

C. Depth distribution of the SON layer

To optimize thermal poling of thin film materials, the first objective is to localize the poling effects within the film, with limited penetration into the substrate. The thickness of the polarized layer depends on both the conductivity properties of the materials (cationic mobility, electronic conductivity) and the poling conditions (temperature, voltage and atmosphere). The influence of applied voltage upon the thickness of the polarized layer was studied by measuring SHG profiles over the cross section of the poled thin film and substrate. Two identical 4 µm thick unannealed Na:Ta_2O_5 films deposited on borosilicate glass were poled by applying a voltage of 1.3 kV to one and 2.0 kV to the other. Fig. 4 shows the SHG profiles of the poled samples. The nonlinear optical (NLO) layer is well confined within the Ta_2O_5 film for an applied voltage of 1.3 kV whereas the use of a higher voltage (2.0 kV) extends the NLO layer into the substrate. Taking into account the spatial resolution of the SHG measurement, the polarized layer thickness is estimated to be 4 and 6 µm for a poling voltage of 1.3 and 2.0 kV, respectively. This preliminary optimization demonstrates that the NLO layer localization can be tuned to be adapted to the film thickness by adjusting the applied voltage.

For the remainder of this study, the applied voltage was fixed at 1.3 kV, allowing the effect of any induced SON in the substrate to be neglected, simplifying the quantification of the efficiency and stability of second-order optical responses of the poled Ta_2O_5 thin films themselves.

D. Maker fringe measurements and SHG stability

Maker fringe analysis has been performed on four different Ta_2O_5 films (annealed and unannealed, with and without the Na additive) of 4 µm thickness, poled at 1.3 kV at 300 °C for 30 minutes. The induced $\chi^{(2)}$ value was determined immediately after the thermal poling treatment by a complete Maker fringe analysis using both angular rotation scans and polarization scans at a fixed angle of incidence. Fig. 5 shows these measurements for the unannealed Na:Ta_2O_5 film. All four sets of experimental data have been fitted to a model based on the optical transfer matrix approach as described in [38], with the refractive indices and the thicknesses of the two layers (substrate and film) taking the values measured above. In fitting the theoretical Maker fringe curves to the experimental data in Fig. 5, we have considered the hypothesis of an electro-optical origin of the induced $\chi^{(2)}$ linked to a frozen-in static electric field along the z axis direction (perpendicular to the anodic glass surface). This would bring about a $C_{\infty v}$ symmetry with a resultant ratio of $\chi^{(2)}_{33}/\chi^{(2)}_{31} = 3$ to describe the second-order optical response of the poled films. As seen in Fig. 5, the agreement between experimental data and calculation is very good, confirming that the SON is due to a frozen-in electric field. Based on the above fitting procedure, the $\chi^{(2)}$ was found to be 0.46±0.02 pm/V for a Na:Ta_2O_5 film and 0.34±0.02 pm/V without the Na additive, in both cases poled at 1.3 kV and 300 °C. Comparing the measurements obtained just after thermal poling on the four samples it was found that for Na:Ta_2O_5 films the effective second-order optical nonlinearity is higher than for Ta_2O_5 thin films. The initial $\chi^{(2)}$ after thermal poling was almost the same whether the samples were annealed or unannealed, for both Na:Ta_2O_5 and Ta_2O_5 films.

The stability of the induced $\chi^{(2)}$ was studied for each sample. The SHG intensity was recorded for a fixed angle of incidence (of -64°) as a function of time after poling. Fig. 6 (a) shows the results from 0 to 50 hours and Fig. 6 (b) shows the results for the full 3000 hours. The lines fitted to the data in Fig. 6 (b) are based on a stretched exponential function [39] shown in Eqn. 1, which is a classical mathematical expression used to describe relaxation phenomena in glassy materials, where t_0 is a delay if the beginning of the experiments is not perfectly defined, τ is the relaxation time, A is the initial magnitude of the SHG signal and β is the exponential power for which a departure from 1 (corresponding to a pure monoexponential behavior) indicates a broadening of the relaxation time distribution.

$$I_{2\omega}(t) = A\exp\left[-\left(\frac{t-t_0}{\tau}\right)^{\beta}\right] \quad (1)$$

This manuscript was accepted by J. Appl. Phys. Click here to see the version of record.

In order to compare SHG signals measured over a long period (more than 1000 hours in our case), it is necessary to take in account any fluctuations in the laser intensity. To this aim, all our SHG data have been normalized to the square of the laser intensity at the fundamental frequency: $I_{2\omega}/I^2_{\omega}$.

For all samples, a fast decrease of the SHG signal is observed during the first three hours after thermal poling. After 50 hours the signal decreases by 23% for the Na:Ta_2O_5 annealed sample, by 35% for the Na:Ta_2O_5 unannealed sample, by 16% for the Ta_2O_5 annealed sample and by 28% for the Ta_2O_5 unannealed sample. The SHG signal decreases faster for Na:Ta_2O_5 thin films than for Ta_2O_5 thin films. For both compositions the SHG signal of unannealed samples decreases faster than the SHG signal of the annealed ones. This trend is confirmed over longer periods (Fig. 6 (b)). The SHG signal of all samples decreases to reach a value close to zero approximatively 12 weeks after the poling treatment.

IV. DISCUSSION

The efficiency of thermal poling is expected to be related to material resistivity and so in the present case, the resistivities of Ta_2O_5 films and glass substrates were measured by impedance spectroscopy at elevated temperature close to the poling temperature. While Na:Ta_2O_5 films exhibited resistivity nearly one order of magnitude lower than Ta_2O_5 films, the strongest second-order optical nonlinearity immediately after poling was induced in these Na:Ta_2O_5 films despite their lower resistivity. This implies that thermal poling effects cannot be simply described by the conduction properties of the materials to be treated. Nevertheless, based on a complete Maker fringe analysis, the $\chi^{(2)}$ tensor of the thermally poled Ta_2O_5 films was shown to have an electro-optic origin referred to as EFISH (electric field induced second harmonic). This enables description of the SON properties of poled Ta_2O_5 amorphous films in terms of the third-order optical susceptibility and the strength of the induced electric field, as described by $\chi^{eff(2)} = 3E_f \chi^{(3)}$. Immediately after poling, $\chi^{(2)}$ was found out to be 0.46±0.02 pm/V and 0.34±0.02 pm/V for an unannealed Na:Ta_2O_5 and Ta_2O_5 film, respectively, poled at 1.3 kV and 300 °C. Using $\chi^{(3)} \approx 11\text{x}10^{-21}$ m^2/V^2 [23] for our Ta_2O_5 thin films, the frozen-in electric field E_f can be estimated to be about 1.0 to 1.4×10^7 V/m. When comparing this with that in other polarized glassy networks it is important to consider only the studies in which the thermal poling treatment was carried out under blocking anodic electrode conditions, as it has been shown that using an open anode the field induced is one order of magnitude lower for the same glassy matrix.[40] Quiquempois et al. [41] reported $\chi^{(2)} = 0.40$ pm/V in silica Infrasil glass ($\chi^{(3)} \approx 2\text{x}10^{-22}$ m^2/V^2) poled under vacuum, Dussauze et al. [40] reported $\chi^{(2)} = 0.3$ pm/V for a soda-lime glass ($\chi^{(3)} \approx 0.6\text{x}10^{-22}$ m^2/V^2) poled under argon atmosphere and 5 pm/V for a phospho-niobate glass ($\chi^{(3)} \approx 5\text{x}10^{-21}$ m^2/V^2).[42] For these three examples, the frozen-in electric field ranges from $0.3\text{x}10^9$ V/m up to $1.6\text{x}10^9$ V/m, which is respectively approximately 20 and 100

times higher than the field strength obtained for Ta_2O_5 films in the present study. In addition, as the thicknesses of the polarized layers reported are similar in all these studies (2-4 µm of thickness), these differences in field strength may be correlated with the uncombined charge density reached in each of these polarized amorphous oxide materials. From our experiments on amorphous Ta_2O_5 films, the charge density can be estimated at 0.77×10^3 Cm^{-3} (considering $\varepsilon_r = 25$ [43], L= 4 µm and $E_f = 1.4 \times 10^7$ V/m) which is about an order of magnitude lower than the charge density evaluated in the thermally poled oxide glasses used for comparison.[40] This indicates that the relatively low second-order optical response measured in these Ta_2O_5 films can be linked to the lower density of uncombined charges which can be sustained by this amorphous matrix.

To explain this observation, charge dissociation processes during the thermal poling treatment must be considered. Poling induces the departure of mobile cations from the depletion region underneath the anode which is partially compensated in the presence of other mobile species, thereby reducing the space charge. In the case of poling under vacuum or in an inert gas, the departure of positive charges is compensated only by the motion of negative charges from the glass network. The nature and conduction mechanisms of these negative charge carriers are still unclear but several hypotheses have been suggested. Oxygen anion motion was first suggested by Carlson.[44, 45] Other studies have noted that molecular oxygen has been observed in polarized glassy matrices, which was explained either by oxidation of the anions and release of electrons [8, 46] or by the formation of peroxide radicals through bond breakage which could then react to form molecular oxygen.[47] However, when the internal electric field reaches a value close to the dielectric breakdown strength, electronic charge carriers play an important role. In this way, the low density of uncombined charges achieved within the thermally poled Ta_2O_5 films may be explained by higher electronic conductivity during the poling process for Ta_2O_5 films as compared to other classical oxides such as silicate glasses. In other words, the activation energy of the compensation mechanism (i.e. negative charge motion) is much lower for Ta_2O_5 films, which lowers the strength of the space charge, limiting the frozen-in field.

The stability of the SHG signal after poling and the influence of prior thermal annealing of the Ta_2O_5 layer upon this was also investigated in this work. It was observed that for both Na:Ta_2O_5 and Ta_2O_5 films the SHG signal from unannealed samples decreases faster than the SHG signal of the annealed samples. The SHG decay curves were found to follow a classical stretched exponential (Eqn.1) similar to the trapping model developed to describe electronic relaxation in amorphous semiconductors where excitons diffuse and recombine at network defects.[39] In the case of the poled Ta_2O_5 films, relaxation starts with the density of uncompensated charges formed during the poling treatment. These can diffuse and reach a "sink", a network defect, which will neutralize these

excitons. At later times, excitons must diffuse over larger distances in order to be neutralized. In the case of an amorphous material the distribution of "traps" or "sinks" within the network is expected to be randomly distributed, resulting in an exponential decay stretched in time as described by the term β deviating from β=1. By fitting the measured SHG decay curves to Eqn. 1 the β values obtained range from 0.65 to 0.75, similar to the results obtained in other amorphous semiconductors [39] and which supports the hypothesis of exciton diffusion within an amorphous network. The fitting procedure also confirms that relaxation times increase significantly with annealing. The two main annealing effects on the properties of amorphous Ta_2O_5 films are (i) a decrease in the refractive index explained by a replenishment of oxygen vacancies in the glass network during annealing and (ii) an increase in the electrical resistivity. These two observations, in the context of a trapping model for electrical charge relaxation, can explain the influence of annealing on (i) the diffusion coefficient of excitons which may be related to the resistivity and on (ii) the number of network defect or "sinks" in the films which may be linked to the oxygen vacancies.

V. CONCLUSION

Second-order optical nonlinearity has been induced in amorphous Ta_2O_5 thin films by thermal poling. The effect of the voltage during the poling on the localization of NLO layer within the thin film was studied and an applied voltage of 1.3 kV was found to produce a symmetrical NLO layer in a 4 μm Ta_2O_5 thin film. Effect of Na addition and annealing on the induced nonlinearity has been studied using Maker fringe analysis. The stability of the induced nonlinearity over 3000 hours has been studied for annealed and unannealed, Na:Ta_2O_5 and Ta_2O_5 samples and the decay mechanisms based on EFISH have been discussed, in addition to comparing the conductivities of these samples at elevated temperatures close to poling temperature. These studies provided useful insight into the decay mechanism in relation with the structural units of the amorphous Ta_2O_5 network and research is underway to optimize the network and stabilize the induced nonlinearity by adding various cations and using a different HMO host. Demonstration of induced nonlinearity in amorphous HMO thin films leads to the realization of electro-optic functionality in planar lightwave circuits especially in the mid-IR paving a way to tunable mid-IR devices such as modulators and on-chip FTIR spectrometers.

ACKNOWLEDGEMENTS

This work is supported by the Programme IdEx Bordeaux – LAPHIA (ANR-10-IDEX-03-02); French Aquitaine region (20121101025), ERC grant agreement no. 291216 "Wideband Integrated Photonics for Accessible Biomedical Diagnostics" and UK EPSRC programme grant, Silicon Photonics for Future Systems (EP/L00044X/1).

REFERENCES

[1]Thomson, A. Zilkie, J.E. Bowers, T. Komljenovic, G.T. Reed, L. Vivien, D. Marris-Morini, E. Cassan, L. Virot, J.M. Fédéli, J.M. Hartmann, J.H. Schmid, D.X. Xu, F. Boeuf, P. O'Brien, G.Z. Mashanovich, and M. Nedeljkovic, Journal of Optics 18, 073003 (2016).
[2]D.J. Moss, R. Morandotti, A.L. Gaeta, and M. Lipson, Nature Photonics 7, 597 (2013).
[3]J.D.B. Bradley, E.S. Hosseini, Purnawirman, Z. Su, T.N. Adam, G. Leake, D. Coolbaugh, and M.R. Watts, Optics Express 22, 12226 (2014).
[4]R.A. Myers, N. Mukherjee, and S.R.J. Brueck, Optics Letters 16, 1732 (1991).
[5]M. Dussauze, E. Fargin, M. Lahaye, V. Rodriguez, and F. Adamietz, Optics Express 13, 4064 (2005).
[6]B. Ferreira, E. Fargin, B. Guillaume, G. Le Flem, V. Rodriguez, M. Couzi, T. Buffeteau, L. Canioni, L. Sarger, G. Martinelli and Y. Quiquempois, J. Non-crystalline Solids 332, 207 (2003).
[7]C. Lasbrugnas, P. Thomas, O. Masson, J. Champarnaud-Mesjard, E. Fargin, V. Rodriguez, and M. Lahaye, Optical Materials 31, 775 (2009).
[8]G. Guimbretière, M. Dussauze, V. Rodriguez, and E.I. Kamitsos, Applied Physics Letters 97, 171103 (2010).
[9]M. Guignard, V. Nazabal, F. Smektala, J. L. Adam, O. Bohnke, C. Duverger, A. Moréac, H. Zeghlache, A. Kudlinski, G. Martinelli and Y. Quiquempois, Advanced Functional Materials 17, 3284 (2007).
[10]R. Jing, Y. Guang, Z. Huidan, C. Guorong, K. Tanaka, K. Fujita, S. Murai, and Y. Tsujiie, Optics Letters 31, 3492 (2006).
[11]H. Zeghlache, M. Guignard, A. Kudlinski, Y. Quiquempois, G. Martinelli, V. Nazabal, and F. Smektala, Journal of Applied Physics 101, 084905 (2007).
[12]M. Dussauze, X. Zheng, V. Rodriguez, E. Fargin, T. Cardinal, and F. Smektala, Optical Materials Express 2, 45 (2011).
[13]A. Lepicard, F. Adamietz, V. Rodriguez, K. Richardson, and M. Dussauze, Optical Materials Express 8, 1613 (2018).
[14]D. Pureur, A.C. Liu, M.J.F. Digonnet, and G.S. Kino, Optics Letters 23, 588 (1998).
[15]O. Sugihara, M. Nakanishi, H. Fujimura, C. Egami and N. Okamoto, JOSA B 15, 421 (1998).
[16]Y. Ren, C. Marckmann, J. Arentoft, and M. Kristensen, IEEE Photonics Technology Letters 14, 639 (2002).
[17]M. Dussauze, A. Malakho, E. Fargin, J.P. Manaud, V. Rodriguez, F. Adamietz, and B. Lazoryak, Journal of Applied Physics 100, 013108 (2006).
[18]M. Abe, T. Kitagawa, K. Hattori, A. Himeno, and Y. Ohmori, Electronics Letters 32, 893 (1996).
[19]X. Cao and S.-L. He, Chinese Physics Letters 20, 1081 (2003).
[20]S. Chao, H.-Y. Chen, Y.-H. Yang, Z.-W. Wang, C.T. Shih, and H. Niu, Optics Express 13, 7091 (2005).
[21]J. Fage-Pedersen, R. Jacobsen, and M. Kristensen, Optics Express 13, 8514 (2005).
[22]J. Fage-Pedersen, R. Jacobsen, and M. Kristensen, Journal of the Optical Society of America B 24, 1075 (2007).
[23]C.-Y. Tai, J.S. Wilkinson, N.M.B. Perney, M.C. Netti, F. Cattaneo, C.E. Finlayson, and J.J. Baumberg, Optics Express 12, 5110 (2004).
[24]N. Li, Purnawirman, Z. Su, E. Salih Magden, P. T. Callahan, K. Shtyrkova, M. Xin, A. Ruocco, C. Baiocco, E. P. Ippen, F. X. Kärtner, J. D. B. Bradley, D. Vermeulen and M. R. Watts, Optics Letters 42, 1181 (2017).
[25]K. Worhoff, J.D.B. Bradley, F. Ay, D. Geskus, T.P. Blauwendraat, and M. Pollnau, IEEE Journal of Quantum Electronics 45, 454 (2009).
[26]A. Aghajani, G. S. Murugan, N. P. Sessions, V. Apostolopoulos and J. S. Wilkinson, Optics Letters 40, 2549 (2015).
[27]A.Z. Subramanian, C.J. Oton, D.P. Shepherd, and J.S. Wilkinson, IEEE Photonics Technology Letters 22, 1571 (2010).
[28]C. Lacava, A. Aghajani, P. Hua, D.J. Richardson, P. Petropoulos, and J. Wilkinson, Proceedings of 2016 Optical Fiber Communications Conference and Exhibition (OFC), Anahein, CA, USA (2016).
[29]C.L. Wu, J.Y. Huang, D.H. Ou, T.W. Liao, Y.J. Chiu, M.H. Shih, Y.Y. Lin, A.K. Chu and C. Lee, Optics Letters 42, 4804 (2017).
[30]M. Belt, M.L. Davenport, J.E. Bowers, and D.J. Blumenthal, Optica 4, 532 (2017).
[31]K. Koskinen, R. Czaplicki, A. Slablab, T. Ning, A. Hermans, B. Kuyken, V. Mittal, G.S. Murugan, T. Niemi, R. Baets, and M. Kauranen, Optics Letters 42, 5030 (2017).
[32]E. Atanassova and A. Paskaleva, Microelectronics Reliability 47, 913 (2007).
[33]J.D.T. Kruschwitz and W.T. Pawlewicz, Applied Optics 36, 2157 (1997).
[34]A.Z. Subramanian, C.J. Oton, J.S. Wilkinson, and R. Greef, Journal of Luminescence 129, 812 (2009).
[35]S. G. Yoon, S. M. Kang and D. H. Yoon, Journal of Optoelectronics and Advanced Materials 9, 1246 (2007).
[36]A. Lepicard, F. Bondu, M. Kang, L. Sisken, A. Yadav, F. Adamietz, V. Rodriguez, K. Richardson, and M. Dussauze, Scientific Reports 8, 1613 (2018).
[37]Q. Lv, M. Huang, S. Zhang, S. Deng, F. Gong, F. Wang, Y. Pan, G. Li and Y. Jin, Coatings 8, 150 (2018).

[38]V. Rodriguez and C. Sourisseau, Journal of the Optical Society of America B 19, 2650 (2002).
[39]J.C. Phillips, Reports on Progress in Physics 59, 1133 (1996).
[40]M. Dussauze, T. Cremoux, F. Adamietz, V. Rodriguez, E. Fargin, G. Yang and T. Cardinal, International Journal of Applied Glass Science 3, 309 (2012).
[41]Y. Quiquempois, N. Godbout, and S. Lacroix, Physical Review A 65, 043816 (2002).
[42]M. Dussauze, E.I. Kamitsos, E. Fargin, and V. Rodriguez, The Journal of Physical Chemistry C 111, 14560 (2007).
[43]V. Macagno and J. W. Schultze, J. Electroanalytical Chemistry and Interfacial Electrochemistry 180, 157, (1984).
[44]D.E. Carlson, Journal of the American Ceramic Society 57, 291 (1974).
[45]D.E. Carlson, K.W. Hang, and G.F. Stockdale, Journal of the American Ceramic Society 57, 295 (1974).
[46]M. Dussauze, V. Rodriguez, A. Lipovskii, M. Petrov, C. Smith, K. Richardson, T. Cardinal, E. Fargin, and E.I. Kamitsos, The Journal of Physical Chemistry C 114, 12754 (2010).
[47]A.V. Redkov, V.G. Melehin, and A.A. Lipovskii, The Journal of Physical Chemistry C 119, 17298 (2015).

Figure Legends:

FIG. 1. Schematic diagram of the thermal poling apparatus

FIG. 2. Dispersion curves of refractive indices of annealed and unannealed, Na:Ta_2O_5 and Ta_2O_5 films obtained by ellipsometry

FIG. 3. XRD measurements of unannealed and annealed a) Ta_2O_5 and b) Na:Ta_2O_5 thin films

FIG. 4. SHG profiles of Na:Ta_2O_5 amorphous thin films on borosilicate substrate poled at 1.3 kV and 2.0 kV

FIG. 5. Experimental and calculated transmitted SHG Maker-fringe patterns for the thermally poled unannealed Na:Ta_2O_5 amorphous thin film, taken at $\theta = -64°$. (a) p-p polarized, (b) s-p polarized, and (c) ψ-p and ψ-s polarized

FIG. 6. Time dependence of the SHG intensity of thermally poled annealed and unannealed Na:Ta_2O_5 and Ta_2O_5 layers on borosilicate glass substrate, measured at -64°

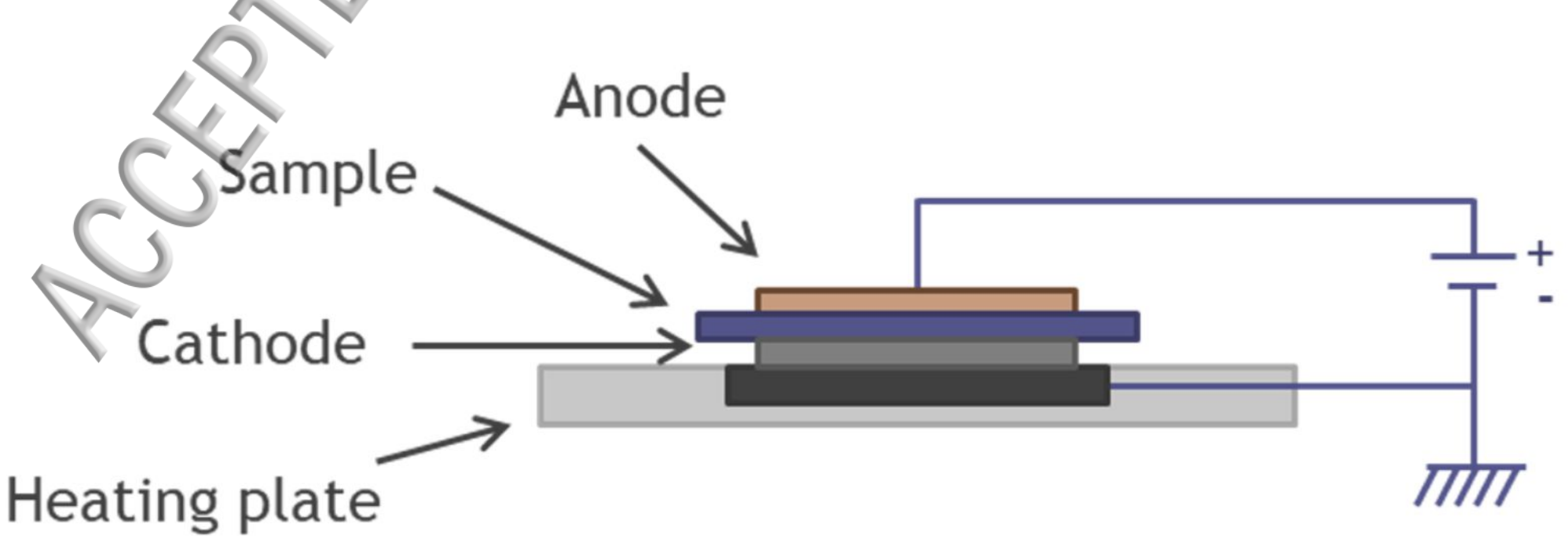

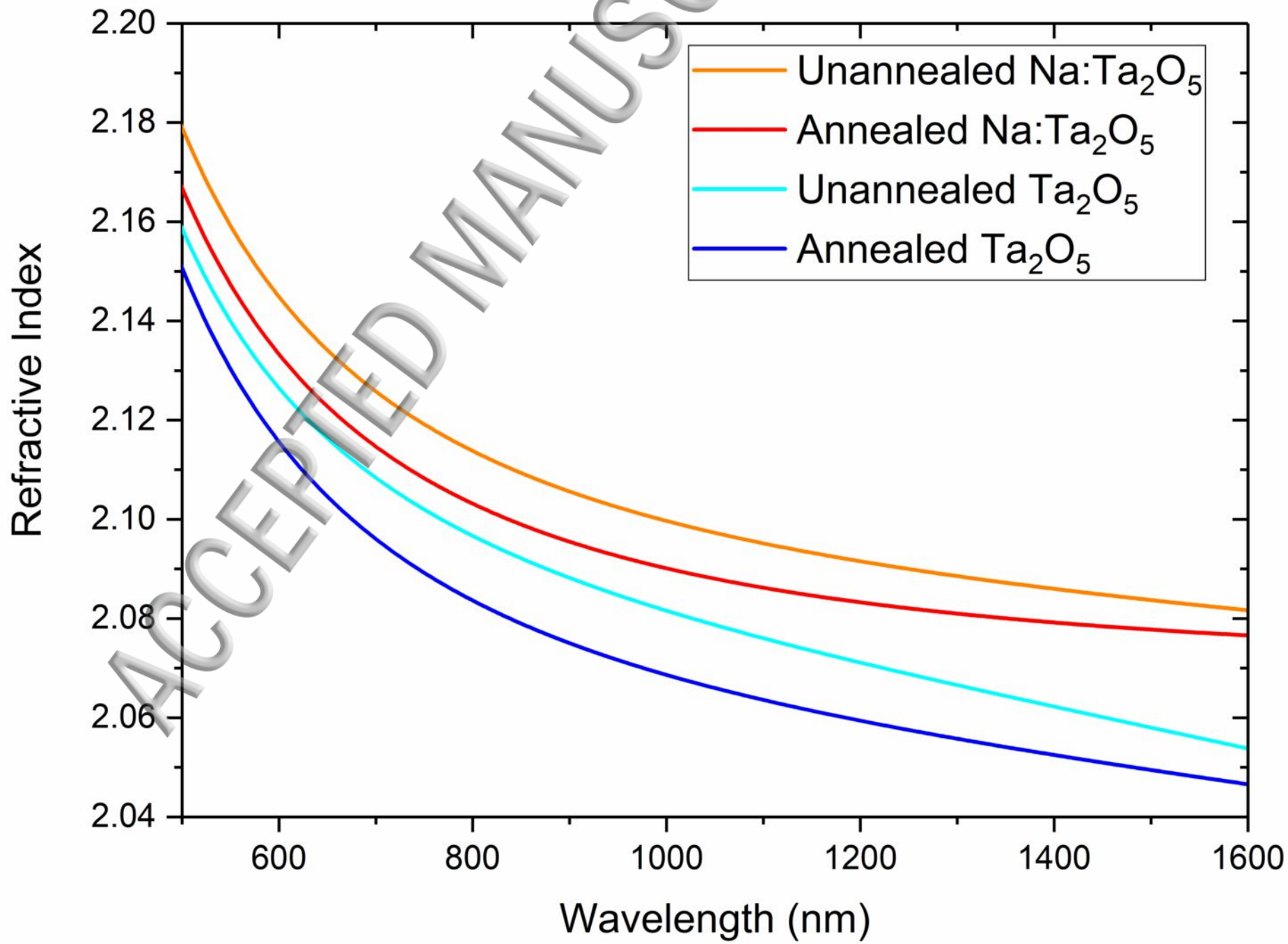

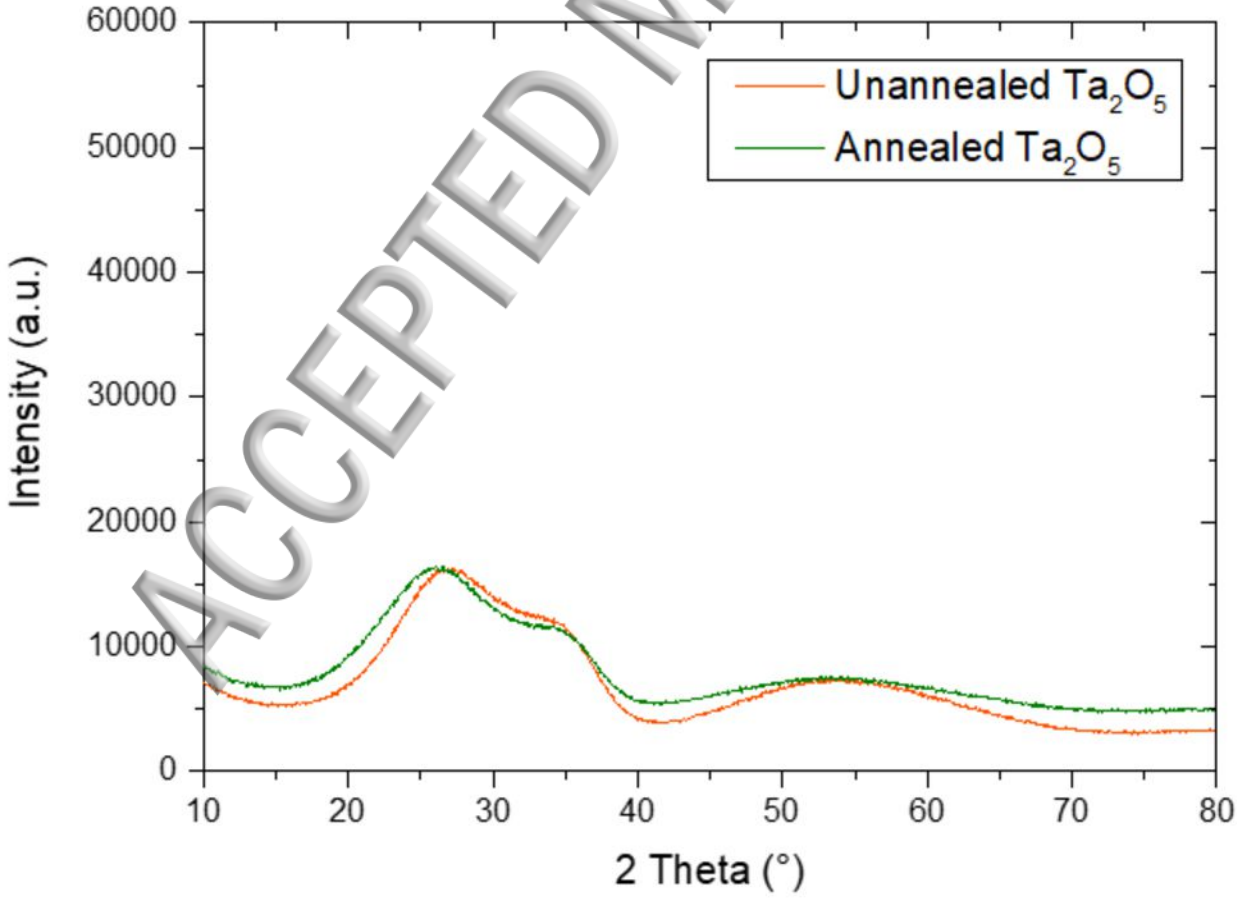

a)

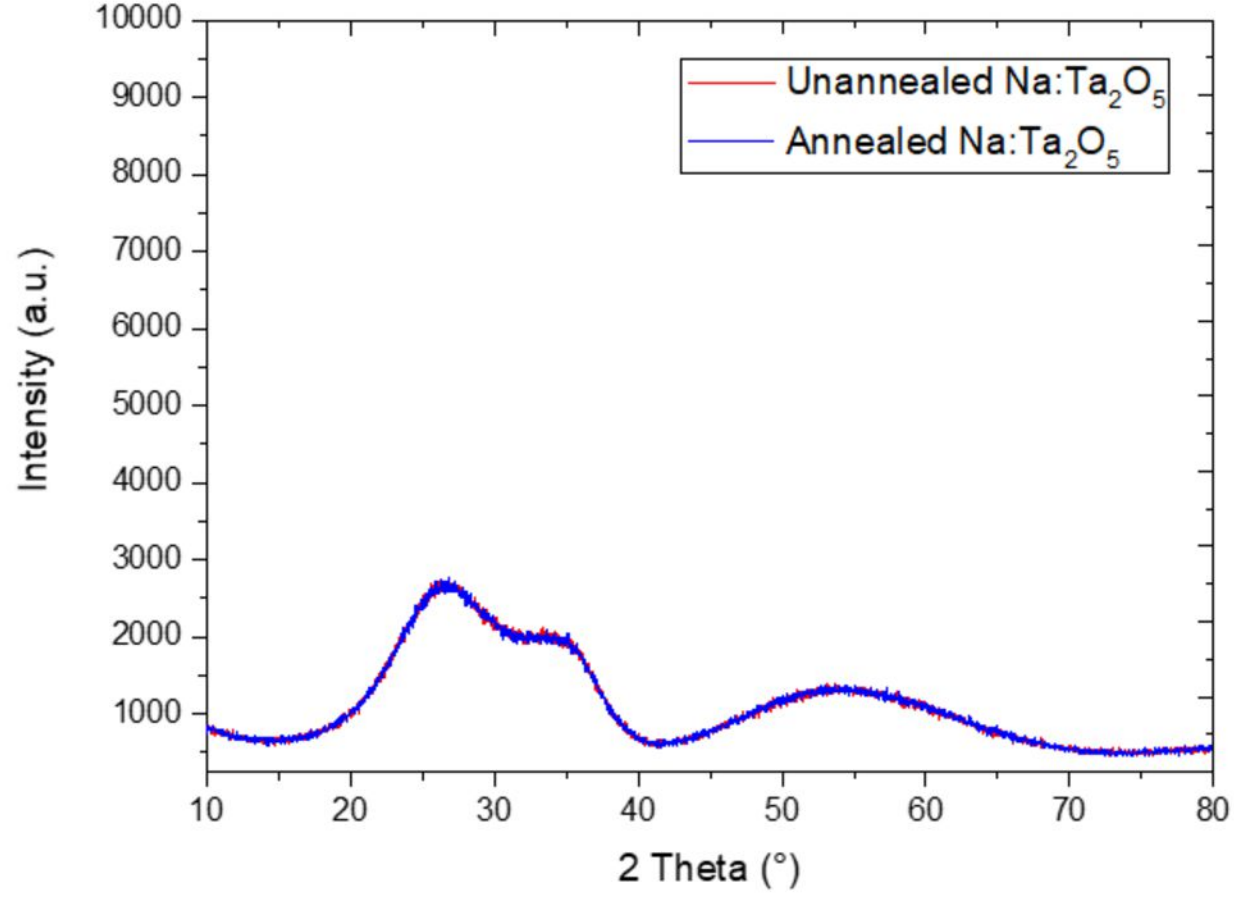

b)

Poling at **1.3 kV**

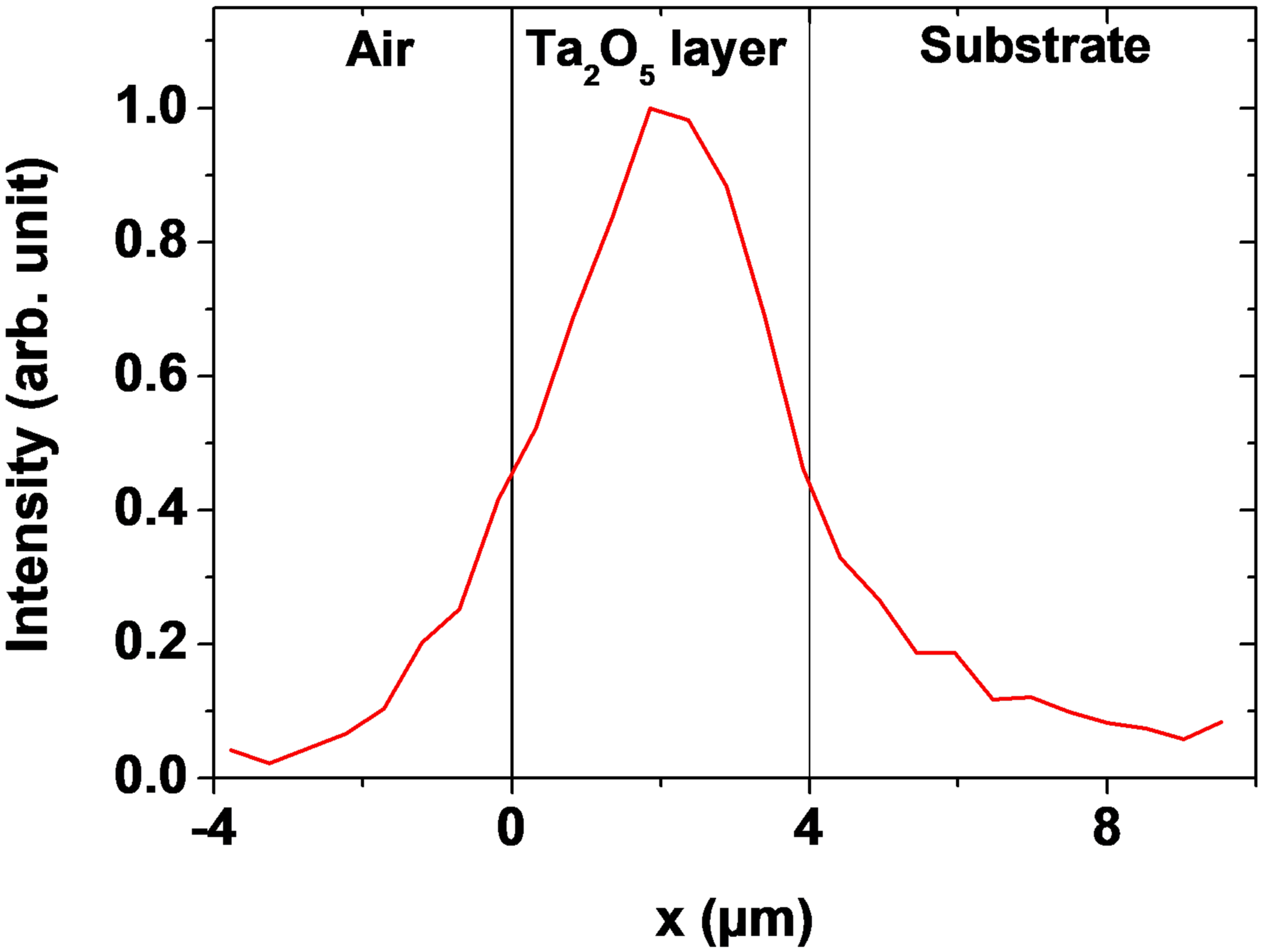

Poling at **2 kV**

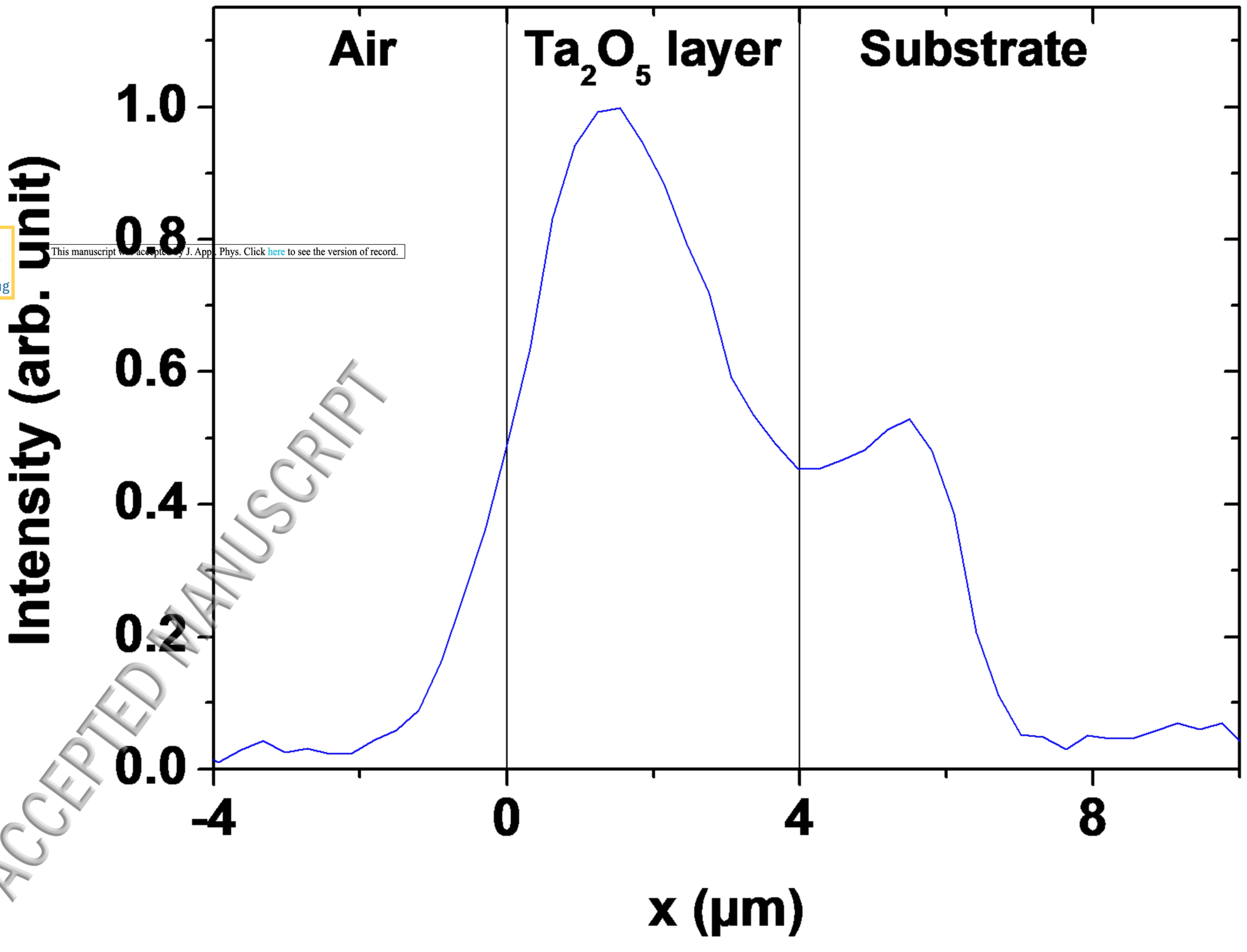

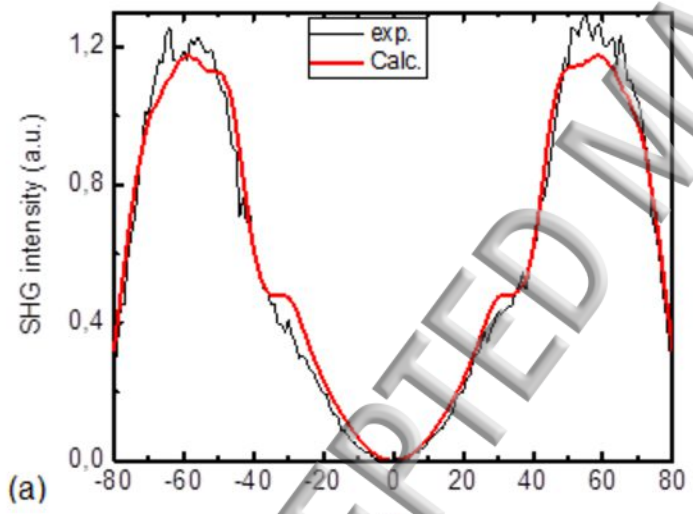

(a)

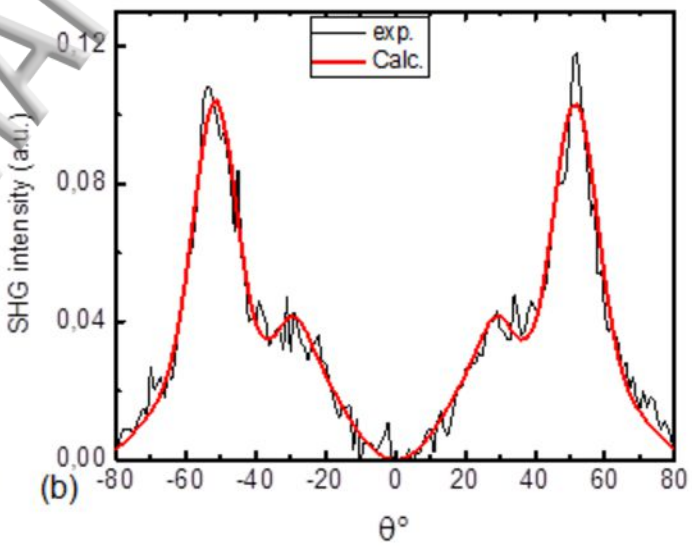

(b)

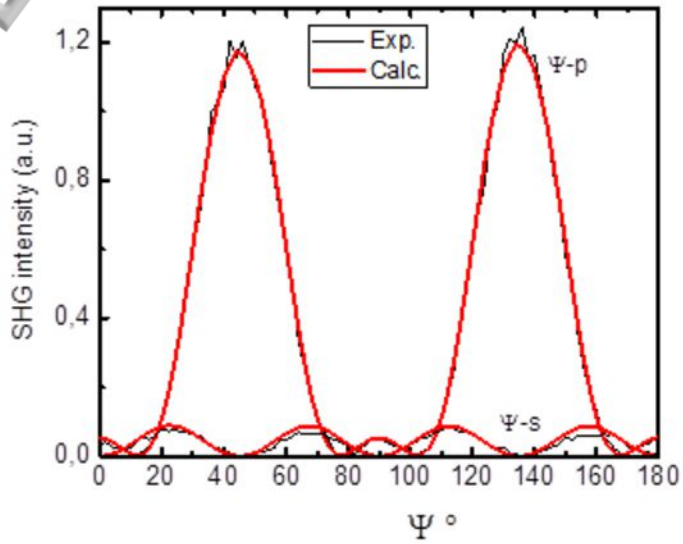

(c)